Supplementary information for

Rate Dependent Structural Changes, Cycling Stability, and Li-Ion Diffusivity in a Layered-Layered Oxide Cathode Material after Prolonged Cycling

Songyoot Kaewmala[a], Wanwisa Limphirat[b], Visittapong Yordsri[c], Jeffrey Nash[d], Sutham Srilomsak [a, f], Aniwat Kesorn [e], Pimpa Limthongkul[f], and Nonglak Meethong [a, g, *]

[a]Institute of Nanomaterials Research and Innovation for Energy (IN-RIE), Research Network of NANOTEC- KKU (RNN), Khon Kaen University, Khon Kaen, 40002, Thailand.
[b]Synchrotron Light Research Institute, 111 University Avenue, Suranaree, Muang, Nakhon Ratchasima, 30000, Thailand.
[c]National Metal and Materials Technology Center (MTEC), National Science and Technology Development Agency, Pathumthani, 12120, Thailand.
[d]The Graduate School, Udon Thani Rajabhat University, Udon Thani, 41000, Thailand.
[e]Optical and Quantum Physics Laboratory, Department of Physics, Faculty of Science, Mahidol University, 10400, Thailand.
[f]National Energy Technology Center (ENTEC), National Science and Technology Development Agency, Pathumthani, 12120, Thailand.
[g]Materials Science and Nanotechnology Program, Department of Physics, Faculty of Science, Khon Kaen University, Khon Kaen, 40002, Thailand.
*Corresponding authors: nonmee@kku.ac.th (NM)

Crystal structure characterization

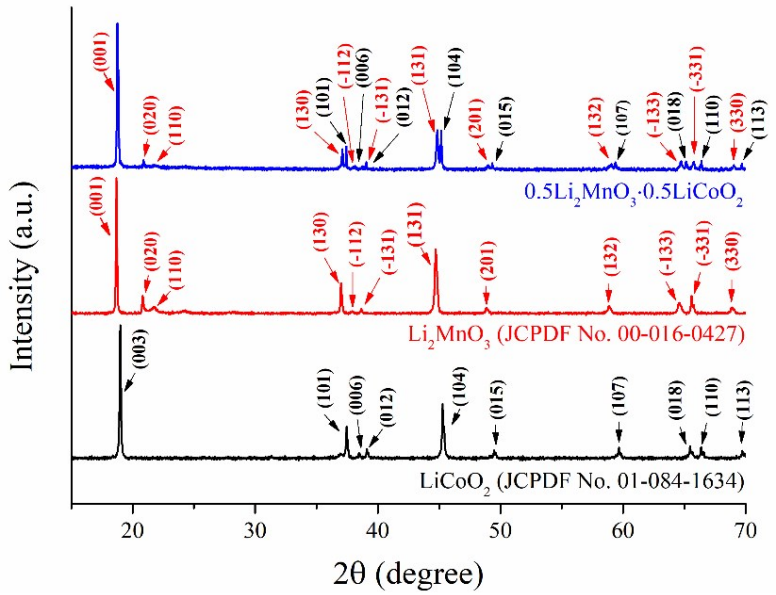

Fig. S1 X-ray diffraction patterns of the $0.5Li_2MnO_3{\cdot}0.5LiCoO_2$, Li_2MnO_3, and $LiCoO_2$ materials

The crystal structure of the prepared $0.5Li_2MnO_3{\cdot}0.5LiCoO_2$ material was investigated using X-ray diffraction (XRD) and the results shown in Fig. S1. The XRD results reveal that prepared sample could be identified as containing both monoclinic Li_2MnO_3 and rhombohedral $LiCoO_2$ phases within the space groups of $C2/m$ and $R\bar{3}m$, respectively. Additionally, weak diffraction peaks were detected in the 2θ range at around 20°-25°. This scenario takes place from the ordering of Li and Mn ions in the transition metal layers of the Li_2MnO_3 component [1-3]. To achieve more detailed information about the structural properties of the prepared material, Rietveld refinements were done using both Li_2MnO_3 and $LiCoO_2$ structural models as presented in Fig. S2. The refined lattice constants are demonstrated in Table S1. The obtained results reflect that the material had quite similar lattice constants with those of pure Li_2MnO_3 and $LiCoO_2$ phases. Moreover, calculated weight factions of Li_2MnO_3 and $LiCoO_2$ phases were 54% and 46%, respectively, corresponding to the required chemical composition of the prepared $0.5Li_2MnO_3{\cdot}0.5LiCoO_2$ material. These results confirm that the prepared material is a composite material.

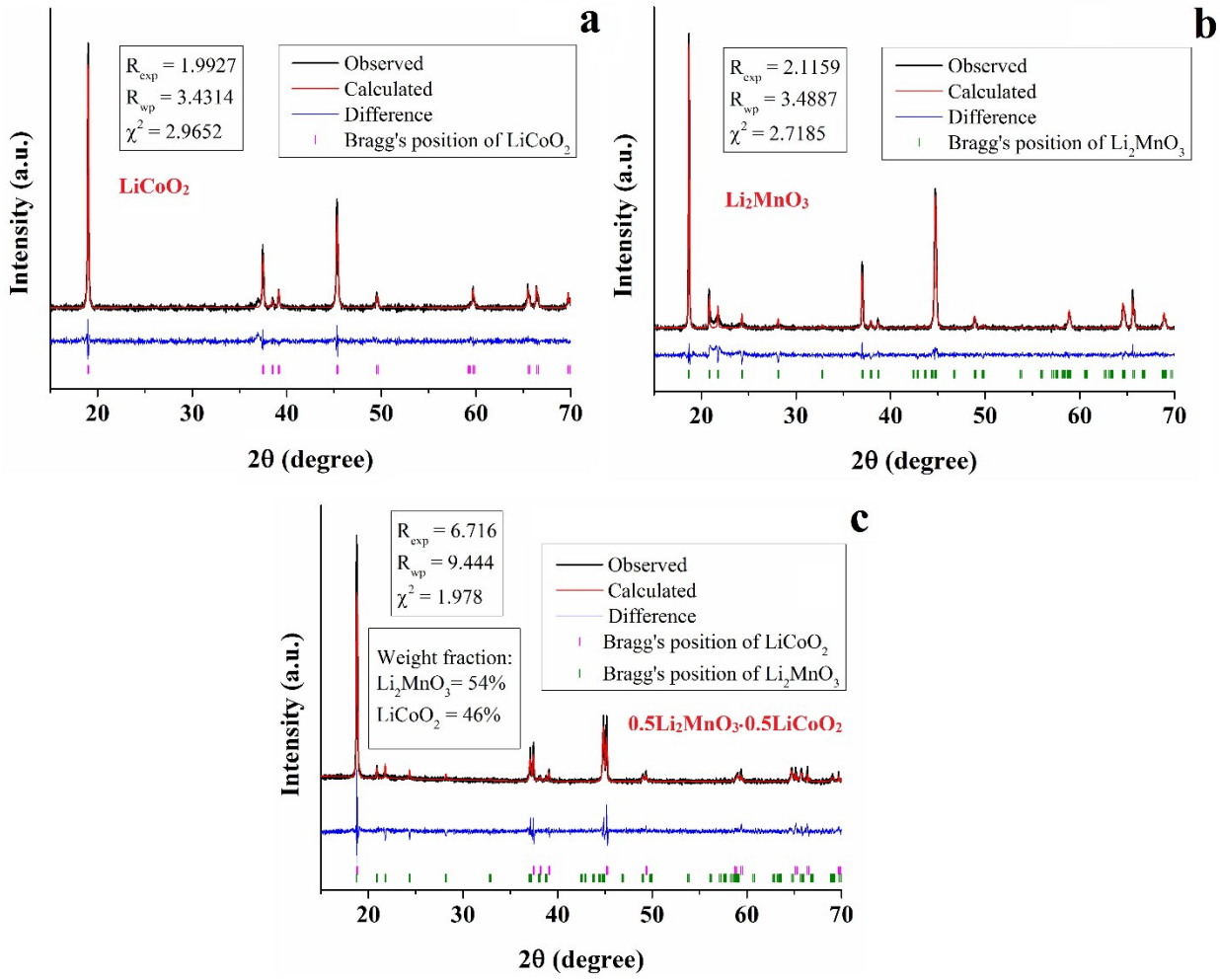

Fig. S2 Rietveld refinement results of pristine $LiCoO_2$ (a), pristine Li_2MnO_3 (b), and the synthesized $0.5Li_2MnO_3{\cdot}0.5LiCoO_2$ (c) materials

Table. S1 Comparisons of the calculated lattice constants of pristine $LiCoO_2$, pristine Li_2MnO_3, and the synthesized $0.5Li_2MnO_3{\cdot}0.5LiCoO_2$ materials

Samples	Lattice parameters							
	Li_2MnO_3 (C/2m) g = a = 90°					$LiCoO_2$ ($R\bar{3}m$) a = b= 90° and g = 120°		
	a (Å)	B (Å)	C (Å)	b (Å)	Unite cell volume (Å³)	a and b (Å)	c (Å)	Unite cell volume (Å³)
$LiCoO_2$	-	-	-	-		2.8158 ±0.0001	14.0523 ±0.0009	96.4903
Li_2MnO_3	4.9262 ±0.0002	8.5276 ±0.0004	5.0236 ±0.0002	109.1952 ±0.0033	199.3000	-	-	-
$0.5Li_2MnO_3{\cdot}0.5LiCoO_2$	4.9301 ±0.0003	8.5099 ±0.0005	5.0111 ±0.0002	109.1829 ±0.0045	198.2788	2.8138 ±0.0001	14.1434 ±0.0006	96.9764

Local atomic structure characterization

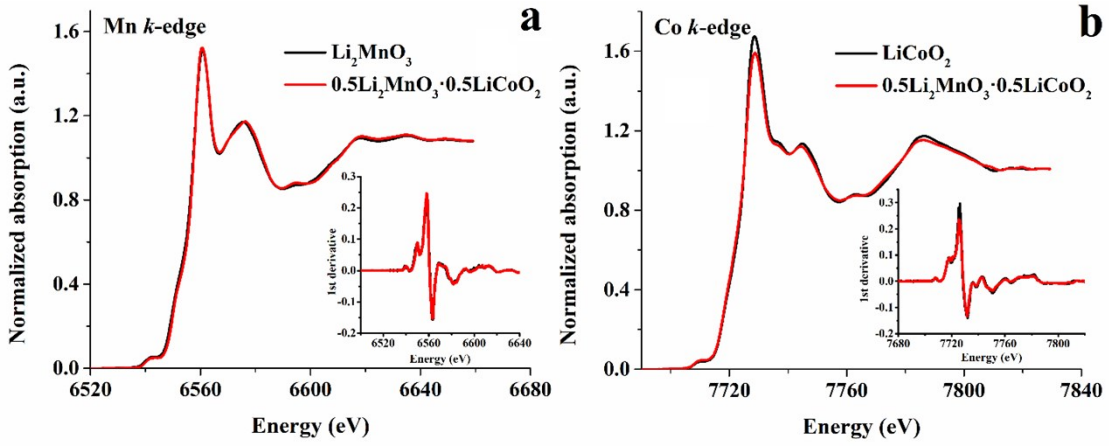

Fig. S3 XANES profiles and the insets revealing the 1st derivative spectra at the Mn (a) and Co (b) *K*-edges of the $0.5Li_2MnO_3{\cdot}0.5LiCoO_2$, Li_2MnO_3, and $LiCoO_2$ materials

The local atomic structure of the prepared $0.5Li_2MnO_3{\cdot}0.5LiCoO_2$ material was elucidated via X-ray absorption spectroscopy (XAS) as demonstrated in Fig. S3. In this experiment, Li_2MnO_3, and $LiCoO_2$ materials were used as standards. The XAS results reveal that the main absorption edge positions for the Mn and Co *K*-edges of the $0.5Li_2MnO_3{\cdot}0.5LiCoO_2$, Li_2MnO_3, and $LiCoO_2$ materials occur at the same position. This scenario is also ensured by the first derivatives of their XANES profiles, as illustrated in the insets of Figs. 3a and 3b. The results indicate that the valence states of the Mn and Co species in the $0.5Li_2MnO_3{\cdot}0.5LiCoO_2$ sample are similar to those of pristine Li_2MnO_3 and $LiCoO_2$. Moreover, the XANES profiles also correspond to those reported in previous works that revealed Mn and Co had valence states of 4+ and 3+, respectively [4-6]. Particularly, the prepared $0.5Li_2MnO_3{\cdot}0.5LiCoO_2$ material provided nearly the same Mn and Co K-edge absorption spectra as those of pristine Li_2MnO_3 and $LiCoO_2$ materials, suggesting that $0.5Li_2MnO_3{\cdot}0.5LiCoO_2$ had the same local atomic structure as those of pristine Li_2MnO_3 and $LiCoO_2$. To obtain more detailed data regarding the local structural properties of the prepared material, EXAFS fittings were performed to calculate the bond lengths of Co-O, Mn-O, Co-TM, and Mn-TM in the synthesized material as presented in Fig. S4. It can be seen that the calculated bond lengths of Co-O and Co-TM in the prepared material are close to those of the pristine $LiCOO_2$ structure for the Co *K*-edge. The calculated bond lengths of Mn-O and Mn-TM in the prepared material are similar to those of the pristine Li_2MnO_3 structure Mn *K*-edge as shown in Table S2. From the experimental results, it can be confirmed that the prepared material is a composite cathode material, corroborated by the HRTEM and XRD results.

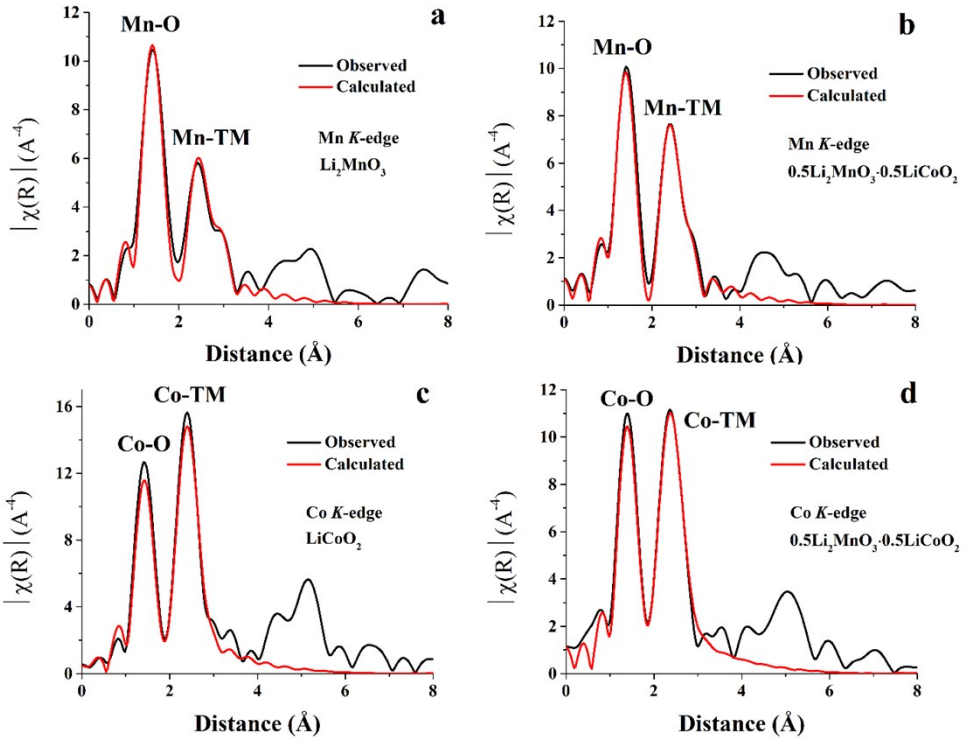

Fig. S4 Mn (a and b) and Co (c and d) *K*-edges EXAFS fitting results of prepared $0.5Li_2MnO_3 \cdot 0.5LiCoO_2$, Li_2MnO_3, and $LiCoO_2$ materials

Table S2. The bond distances and agreement indices obtained from XAS spectra fitting of EXAFS spectra of pristine $LiCoO_2$, pristine Li_2MnO_3, and the synthesized $0.5Li_2MnO_3 \cdot 0.5LiCoO_2$ materials

Li_2MnO_3 structure (Mn *K*- edge)						
Sample	Shell	N (atoms)	R (Å)	σ^2 (Å²)	R-factor	E_0 (eV)
Li_2MnO_3	O	6	1.891 ±0.012	0.002 ±0.001	0.018	-4.017
	Mn	3	2.844 ±0.016	0.002 ±0.001		
$0.5Li_2MnO_3 \cdot 0.5LiCoO_2$	O	6	1.891 ±0.019	0.004 ±0.001	0.016	-4.886
	Mn	3	2.837 ±0.017	0.002 ±0.002		
$LiCoO_2$ structure (Co *K*-edge)						
Sample	Shell	N (atoms)	R (Å)	σ^2 (Å²)	R-factor	E_0 (eV)
$LiCoO_2$	O	6	1.907 ±0.015	0.003 (set)	0.020	-4.505
	Co	6	2.816 ±0.017	0.004 (set)		
$0.5Li_2MnO_3 \cdot 0.5LiCoO_2$	O	6	1.911 ±0.014	0.004 (set)	0.008	-4.488
	Co	6	2.817 ±0.013	0.004 (set)		

Electrochemical characterization

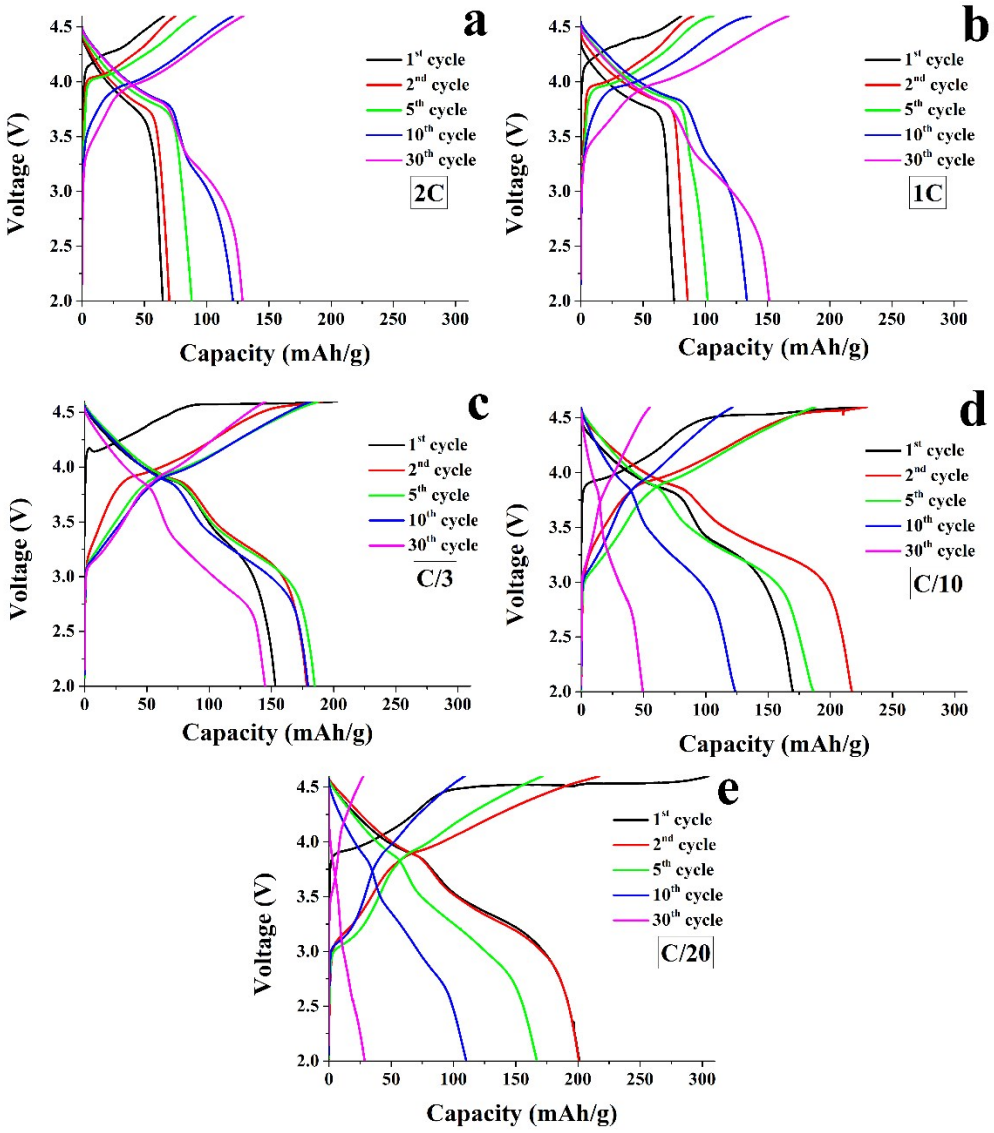

Fig. S5 Voltage profiles of a $0.5Li_2MnO_3 \cdot 0.5LiCoO_2$ sample cycled using various current rates of 2C (a), 1C (b), C/3 (c), C/10 (d), and C/20 (e) rates

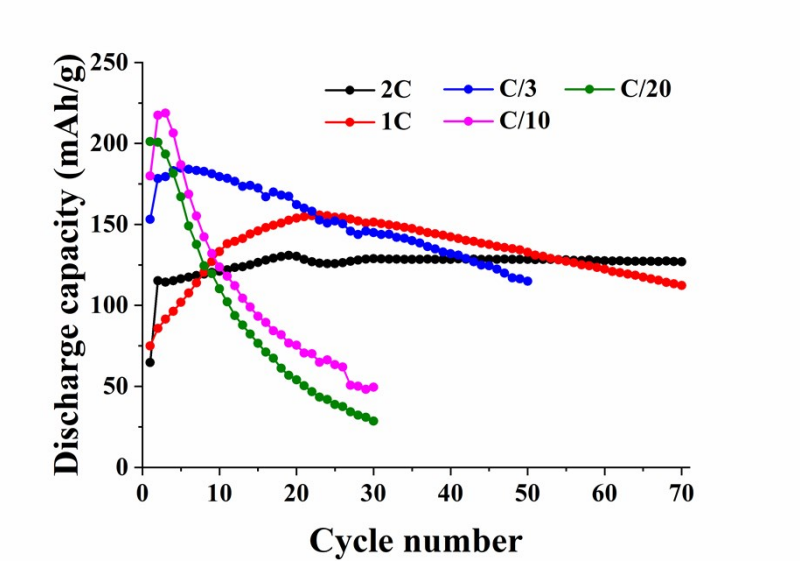

Fig. S6 Cycling performance of a $0.5Li_2MnO_3 \cdot 0.5LiCoO_2$ sample cycled at various current rates of 2C, 1C, C/3, C/10, and C/20

From these results, different cycling performance of electrodes cycled at various C-rates is apparent. In the case of cycling at slow rates (C/20, C/10, and C/3), most of the Li_2MnO_3 component was activated after the first few charge-discharge cycles and subsequently induced a large degree of a spinel phase transition and structural degradation. This causes high capacity fading after the first few cycles. When the electrode was cycled at 1C, most of the Li_2MnO_3 component is activated (a large activation) after about 20 cycles. During this progressive Li_2MnO_3 activation, the capacity during the first 20 cycles continuously increases. After that, the capacity decreases significantly due to a large degree of a spinel phase transition and structural degradation. In the case of the electrode cycled at 2C, the Li_2MnO_3 component was only slightly activated, leading to a small but gradually increased capacity. Li_2MnO_3 activation and capacity increases continuously until most of the Li_2MnO_3 phase is completely activated after a much greater number of cycles than electrodes cycled at slower rates, as presented in Fig. S6. The results reveal that the current rate significantly affects the degree of Li_2MnO_3 activation during cycling, altering structural transition behaviors during electrochemical cycling and the electrochemical properties of the material.

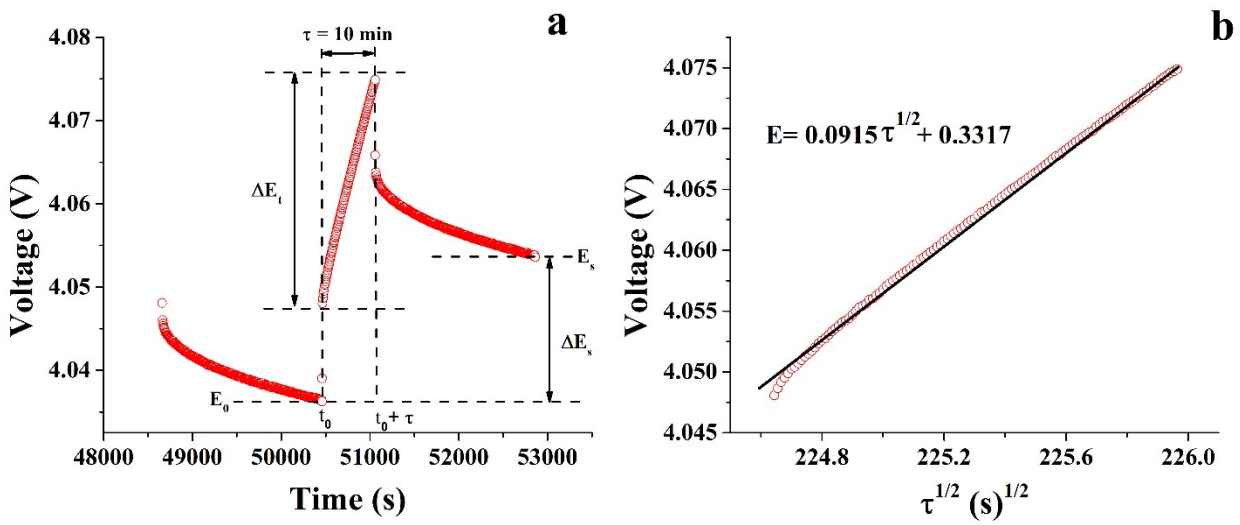

Fig. S7 Single titration at about 4.05 V during GITT measurement (a) and the cell voltage as a function of $t^{1/2}$ (b)

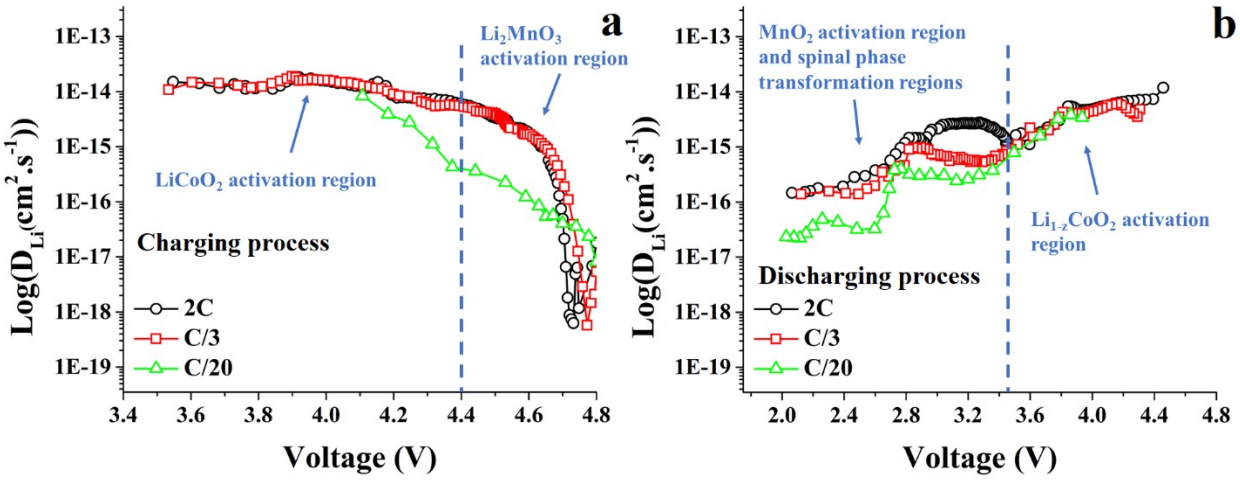

Fig. S8 Calculated lithium ion diffusion coefficients as a function of cell voltage during charging (a) and discharging (b) of the $0.5Li_2MnO_3 \cdot 0.5LiCoO_2$ materials cycled at 2C, 1C, and C/20 rates after 30 cycles

Table. S3 Comparison of calculated resistances obtained from fitting parameters using the equivalent circuit model illustrated in Fig. S9 of the fresh cell and the cells cycled at various current rates after 30 cycles

Sample	R_W (W)	R_{CT} (W)
Fresh cell	0.428	38.60
2C	0.521	75.83
C/3	0.515	83.33
C/20	0.530	168.42

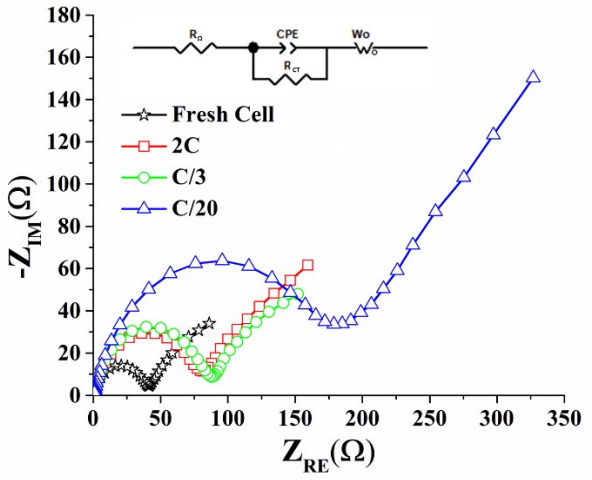

Fig. S9 Nyquist plots of the fresh cell and the cells cycled at 2C, 1C, and C/20 after cycling for 30 cycles and the inset shows an equivalent circuit. R_W, R_{CT}, CPE, and W_0 denote the ohmic resistance, the charge transfer resistance, constant phase element, and Warburg resistance, respectively.

References

1. J. Bréger, M. Jiang, N. Dupré, Y. S. Meng, Y. Shao-Horn, G. Ceder and C. P. Grey, *Journal of Solid State Chemistry*, 2005, **178**, 2575-2585.
2. F. Amalraj, D. Kovacheva, M. Talianker, L. Zeiri, J. Grinblat, N. Leifer, G. Goobes, B. Markovsky and D. Aurbach, *Journal of The Electrochemical Society*, 2010, **157**, A1121.
3. W. C. West, J. Soler and B. V. Ratnakumar, *Journal of Power Sources*, 2012, **204**, 200-204.
4. B. R. Long, J. R. Croy, F. Dogan, M. R. Suchomel, B. Key, J. Wen, D. J. Miller, M. M. Thackeray and M. Balasubramanian, *Chemistry of Materials*, 2014, **26**, 3565-3572.
5. J. Bareño, M. Balasubramanian, S. H. Kang, J. G. Wen, C. H. Lei, S. V. Pol, I. Petrov and D. P. Abraham, *Chemistry of Materials*, 2011, **23**, 2039-2050.
6. J. R. Croy, M. Balasubramanian, D. Kim, S.-H. Kang and M. M. Thackeray, *Chemistry of Materials*, 2011, **23**, 5415-5424.